RSC Advances

ROYAL SOCIETY OF CHEMISTRY

www.rsc.org/advances

Enhanced non-linear viscoelastic properties of TATB-based polymer bonded explosives filled with hybrid graphene/multiwalled carbon nanotubes

Congmei Lin, Guansong He, Jiahui Liu, Zhong Huang, Liping Pan, Jianhu Zhang, Shijun Liu *

ABSTRACT: In this work, hybrid graphene/multiwalled carbon nanotubes (MWCNTs) nanofillers were selected to improve to non-linear viscoelastic properties of 1,3,5-triamino-2,4,6-trinitrobenzene (TATB)-based polymer bonded explosive (PBX). The morphology, mechanical properties, and creep behaviors of TATB-based formulations were studied. The results were compared with the corresponding composites with individual graphene nano-additives. Scanning electron microscopy observation results indicated graphene particles were fairly well dispersed in the nanocomposite filled with hybrid graphene/MWCNTs, while graphene sheets were prone to aggregation in the PBX filled with individual graphene. Hybrid graphene/MWCNTs modified PBX exhibited higher storage modulus in the whole temperature range. The compressive fracture energy (W_c) and tensile fracture energy (W_t) at 20 °C are up to 31.6% and 89.6% higher than that of PBX without nanofillers. The creep responses of the composites were determined by short-time creep tests at various temperatures and stresses. The creep compliance curve for TATB-based PBXs shows a remarkable synergetic effect between graphene and MWCNTs in improving the creep resistance. The better dispersion of graphene nanoparticles and higher interfacial zones, which produced strong interfacial interaction between the graphene and polymer matrix to restrict the mobility of polymer chains, were considered as crucial factors for the improvement in the creep resistance for TATB-based PBXs.

1. Introduction

It is well known that as a monolayer of sp^2-hybridized carbon atoms arranged in a two-dimensional lattice, graphene is a nanomaterial of considerable interests for a variety of applications[1-3]. Owing to the exceptional thermal, mechanical, and electrical properties, i.e. tensile strength (100 GPa) and modulus (1 TPa), 25% elongation at break, and excellent thermal (> 3000 W/m·K) and electric (6000 S/cm) conductivity, graphene is favorable to prepare polymer composites[4-7].

During storage, transportation, and usage, polymers are subject to various loads and prone to deformation and damage. As a time-dependent mechanism of plastic deformation, creep is the most basic representation of static viscoelasticity and one of the main failure forms of polymer material. Considering the disadvantages, increasing attention has being paid to improving the creep resistance of polymers[8-14]. One effective way is the addition of very low content of graphene[15-18]. Zandiatashbar et al.[15] have investigated the creep behavior of epoxy–graphene platelet (GPL) nanocomposites by macroscopic testing and nanoindentation. It is revealed that the

* Institute of Chemical Materials, China Academy of Engineering Physics, Mianyang, Sichuan 621900, P. R. China. E-mail: lsj99@sohu.com; Fax: +86-816-2495856; Tel: +86-816-2489302.

nanocomposite with 0.1 wt% GPLs creeps significantly less than the unfilled polymer at elevated stress and temperature. Incorporation of chemically reduced graphene oxide (CRGO) into PS polymer is also found to significantly improve the creep resistance and recovery properties[16]. The role of CRGO on improving the creep and recovery performance of thermoplastics is proposed and discussed based on the analytical modelings (Burger's model and Weibull distribution function) and experimental results[17].

However, there are strong limitations for the application of graphene in the design and fabrication of polymer composites. These limitations are caused by the aggregation and stacking of graphene sheets, due to the large Vander Waals forces and strong π-π interactions between graphene planar nanosheets[19,20]. Therefore, improving the dispersion of graphene in the nanocomposites is of great interest. A typical approach to reduce the aggregation of graphene is acid oxidation. However, the severe, complex reaction conditions and the damage of the graphitic structure have been considered to be a hindrance of the application for acid oxidations[21-24]. Up to now, great efforts have been devoted to study the effects of hybrid graphene/carbon nanotubes (CNTs) on the inhibition of the graphene aggregation. Due to that stacking of individual two-dimensional multi-graphene platelets (MGPs) is effectively inhibited by introducing one-dimensional multiwalled carbon nanotubes (MWCNTs), a remarkable synergetic effect between the MGPs and MWCNTs in improving the mechanical properties and thermal conductivity of epoxy composites is demonstrated[25]. Araby et al.[26] have developped elastomer/graphene platelet/MWCNT (3-phase) composites by hybridizing the graphene platelets (GnPs) and MWCNTs through melt compounding. At a total filler content of 26.7 vol%, the tensile strength, Young's modulus and tear strength of the 3-phase composites respectively increase by 707%, 825% and 428% in comparison with 404%, 710% and 270% for the 2-phase composites wherein only GnPs are used. Self-assembled graphene/carbon nanotube (CNT)/polystyrene hybrid nanocomposites have been prepared by water-based in situ microemulsion polymerization[27]. It has been found that an admixture of the two types of carbon fillers provides better improvement in the thermal and mechanical properties compared to the neat polymer.

1,3,5-triamino-2,4,6-trinitrobenzene (TATB)-based polymer bonded explosive (PBX) is a kind of particle highly-filled polymer composite and has attracted increasing attention in recent years[28-31]. Incorporation of graphene and MWCNTs into polymeric materials has been widely investigated over the past decades. However, less attention is paid to the effects of hybrid graphene/MWCNTs on the non-linear viscoelastic properties of TATB-based PBX. In the present research, a strategy was designed to improve the mechanical properties of TATB-based PBX filled by 1-D MWCNTs and 2-D graphene. In addition, morphological characterization was carried out to study the failure mechanism of PBXs and the dispersion of graphene in the nanocomposites.

2. Experimental

2.1 Materials

Graphene and multiwalled carbon nanotubes (MWCNTs), purchased from Beijing DK Nano Technology Co., Ltd. China, were used as reinforcements. The raw material of graphene with 1-5 μm in length and 0.9 nm to 1.2 nm in thickness was used as received. The outer diameter and length of MWCNTs were less than 8 nm and approximately 50 μm, respectively. The specific surface area of graphene and MWCNTs were more than 500 and 350 m^2/g, respectively. The

properties of graphene and MWCNTs were provided from the Beijing DK Nano Technology Company. The appearance of graphene and MWCNTs was observed using a scanning electron microscope (SEM), as shown in Fig. 1. TATB (purity 99 %, particle size about 17 μm) was provided by Institute of Chemical Materials, CAEP, China. Fluoropolymer used as polymer binder in this work was a copolymer of chlorotrifluoroethylene and vinylidene fluoride, obtained from Zhonghao Chenguang Chemical Industry Co., Ltd. China.

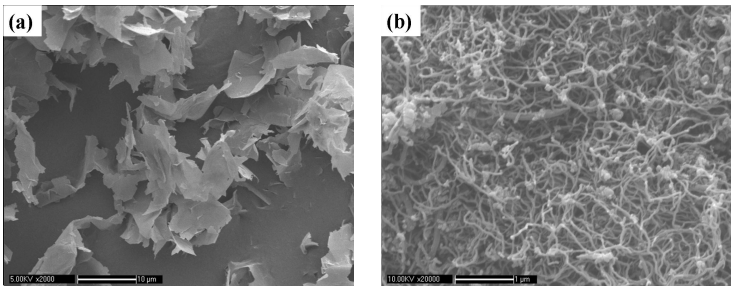

Fig. 1 SEM images of (a) graphene and (b) MWCNTs.

2.2 Sample preparation

The fluoropolymer was firstly dissolved with the mixed solvent of ethyl acetate and butyl acetate by mechanical stirring for 12 h. Then, TATB (180 g) was added to H_2O (180 mL) and dispersed whilst stirring at 70 °C in a vacuum. The polymer binder solution was added dropwise. After removing the organic solvent, the molding powders of TATB-based formulations were prepared. The molding powders were dried in an oven at 60 °C for 12 h to remove moisture. The composite was manufactured into test specimens for testing by hot press at 120 °C under a pressure of about 300 MPa. A reference TATB-based PBX without nanofillers was labeled as PBX-A. Graphene/MWCNTs modified composite was also processed by the same methods, labeled as PBX-B. The weight content of graphene and MWCNTs in PBX-B were 0.1% and 0.05% by weight, respectively. For comparison, the PBX with only 0.15% by weight graphene (PBX-C) was also tested. For PBX-B or PBX-C, graphene/MWCNTs composites or graphene were added firstly to a fluoropolymer solution with ethyl acetate and butyl acetate as solvent and dispersed with ultrasound vibration for 15 min. Then the fluoropolymer solution with graphene/MWCNTs composites or graphene was added dropwise to the TATB and H_2O mixture.

2.3 Measurements

Morphological measurements were performed with a SEM at an operating voltage of 5-10 kV.

Raman analysis was conducted with DX2smart Raman spectrometer (USA).

Mechanical tests were performed with a universal testing machine 5582 (INSTRON, USA) at ambient temperature and elevated temperature. The specimens of explosive pellet with dimensions of ϕ 20 mm × 20 mm and ϕ 20 mm × 6 mm (diameter × height) for compressive and Brazilian tests were molded at 120 °C. Each test was repeated on three to five samples. Average observations were reported.

Dynamic mechanical analysis (DMA) was conducted with the help of a DMA 242C apparatus (Netzsch, Germany) in three-point bending mode at a frequency of 1 Hz. For each test, the heating rate was set to 1 °C/min. The fracture surfaces of the composite explosives under flexural loading were comparatively examined and analyzed by a SEM.

Rectangular specimens with dimensions of 30 mm × 10 mm × 1~2 mm (length × width ×

thickness) were made for the creep tests. A DMA 242C apparatus (Netzsch, Germany) in three-point bending mode was used to measure deformation as a function of time under a constant stress level. The tests were carried out at four temperatures from 30 to 80 °C and three stress levels from 4 to 9 MPa for 5400 s.

3. Results and discussion

3.1 Raman analysis

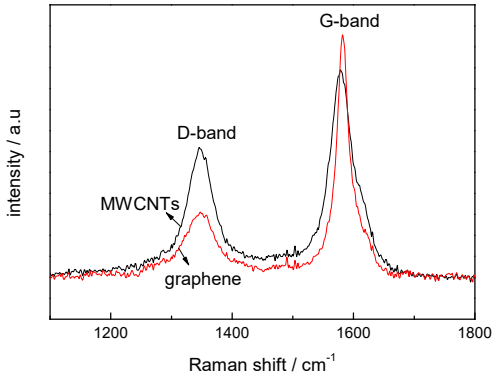

Fig. 2 Raman spectra of graphene and MWCNTs.

The graphitic structures of graphene and MWCNTs are characterized by Raman spectra, as displayed in Fig. 2. Both graphene and MWCNTs contain D band and G band centered at 1347 and 1582 cm^{-1}, respectively, in accordance with the results as reported earlier[25]. The D band is corresponding to the defects in the disorder-induced modes (or sp^3-hybridized carbons). And the G band belongs to in plan bond-stretching motion of the pairs of C sp^2 atoms[32,33]. However, the integrated area ratio of D band and G band (I_D/I_G) for these two materials show an obvious difference. The I_D/I_G ratio for graphene is observed to be 0.583, which is much smaller than that of MWCNTs (0.784), indicating a higher crystalline structure. The better structure quality of graphene results in higher mechanical properties than MWCNTs.

3.2 Mechanical properties

The relaxation processes in polymer composites that are responsible for viscoelastic behavior could be revealed by dynamic mechanical measurements. The storage modulus (E') and loss factor (tanδ) curves over a temperature range of 0-100 °C for the TATB-based PBXs studied here are shown in Fig. 3. Comparing PBX-A without nanofillers, the storage modulus is improved for PBX-B in the whole temperature range. A relaxation process is evident as an abrupt decline in storage modulus plots and a peak in loss modulus plots at the temperature around 50 °C. The relaxation process is attributed to the glass-to-rubber transition of the amorphous phase for the fluoropolymer binder[28]. As demonstrated in Figure 3b, graphene/MWCNTs composite or graphene has obvious effects on the PBX's dynamic mechanical properties. The expected improvement in the glass transition temperature derived from the restriction of molecular motion for polymer binder with the addition of graphene/MWCNTs composites or graphene is observed.

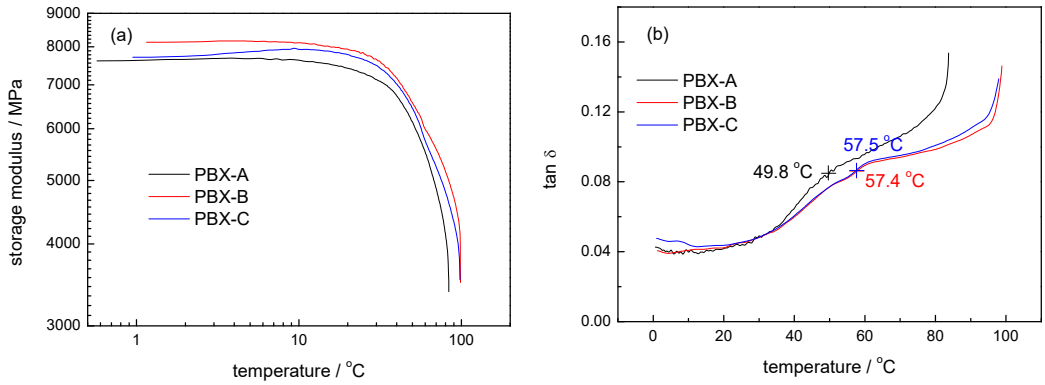

Fig. 3 Dynamic mechanical (a) storage modulus and (b) tanδ as a function of temperature for TATB-based PBXs.

Compressive and Brazilian test were conducted at room temperature and an elevated temperature of 60 °C to compare the mechanical response of PBX-A and PBX-B. Fig. 4 reveals the representative stress-strain curves of two PBXs. It can be seen that the compressive and tensile strength are slightly enhanced for PBX-B, compared with that of PBX-A. The compressive elongation at break at 20 and 60 °C and tensile elongation at break at 20 °C are raised by 29.6%, 37.8%, and 54.2% compared to PBX-A, when hybrid graphene/MWCNTs is used.

The impact toughness (A_k) and the fracture toughness (K_{IC}) are main parameters to characterize the fracture toughness of the engineering materials. In order to solve the limits of A_k and K_{IC} in characterization of explosive fracture toughness, the tensile fracture energy (W_t) and the compressive fracture energy (W_c) based on the stress-strain curve have been put forward by Wen et al.[34] The similarity between the physical meanings of the fracture energy parameters (W_t, W_c) and the impact toughness A_k, was found via analyzing the test principle although they could not be directly measured. W_t, W_c and K_{IC} for different explosives at a series of temperatures were studied by experiments. Results show that the W_t, W_c and K_{IC} of explosives have the same change trend whether for different type explosives or at different temperatures, which indicates they can be used to characterize the toughness of explosive materials[34]. Therefore, W_t and W_c are chosen to characterize the fracture toughness of TATB-based PBXs. According to Wen et al.[34], the W_t and W_c could be obtained by the integration of the stress-strain curve and can be calculated as:

$$W_t = \int_0^{\varepsilon_b} \sigma_t(\varepsilon) d\varepsilon \quad (1)$$

$$W_c = \int_0^{\varepsilon_b} \sigma_c(\varepsilon) d\varepsilon \quad (2)$$

where σ_t denotes tensile stress, σ_c denotes compressive stress, ε is the tensile or compressive strain, ε_b is the strain at the maximal tensile or compressive stress, respectively. Fig. 5 gives the W_t and W_c values for TATB-based PBXs at room temperature and elevated temperature. PBX-B has up to 31.6%, 34.9%, and 89.6% higher W_c at 20 and 60 °C and W_t at 20 °C than PBX-A, suggesting that PBX could be toughened by the addition of hybrid graphene/MWCNTs. According to the definition, the fracture energy represents the absorbed energy per unit volume before sample starts to crack. Therefore, the addition of 0.15% hybrid graphene/MWCNTs gives rise to a better crack resistance.

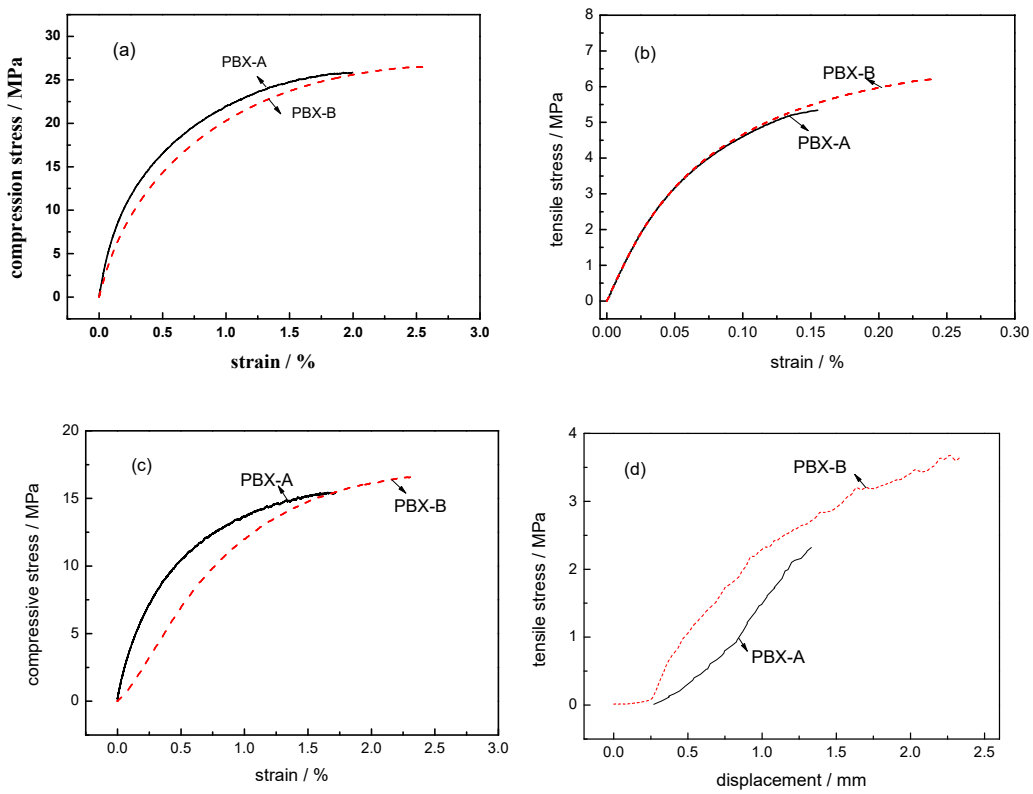

Fig. 4 The typical mechanical response for TATB-based PBXs at room temperature and elevated temperature: (a) compressive test at room temperature, (b) Brazilian test at room temperature, (c) compressive test at 60 °C, (d) Brazilian test at 60 °C.

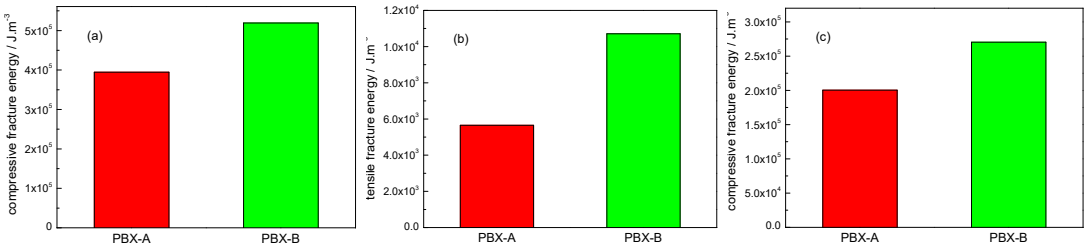

Fig. 5 The fracture energy for TATB-based PBXs at room temperature and elevated temperature: (a) compressive fracture energy at room temperature, (b) tensile fracture energy at room temperature, (c) compressive fracture energy at 60 °C.

3.3 Morphological observation

The SEM micrographs of the fracture surface for TATB-based PBXs without and with hybrid graphene/MWCNTs obtained after dynamic mechanical measurements are shown in Fig. 6a and 6b. It can be clearly seen that a lot of filamentous binder exist at the fracture surface of two PBXs, indicating that the rupture mode is mainly binder breakage and the microscopic fracture mechanism would not change by the incorporation of hybrid graphene/MWCNTs. However, it should be emphasized that the amount and magnitude of filamentous binder evidently increase in the presence of hybrid graphene/MWCNTs. The results are attributed to the fact that the interfacial interaction between hybrid graphene/MWCNTs particles and binder matrix is strongly enhanced

for PBX-B, resulting in a better stress transfer from polymer matrix to nanoparticles and more binder breakage under combined temperature and force loading.

In order to characterize the distribution state of hybrid graphene/MWCNTs particles in the polymer matrix, graphene/MWCNTs/fluoropolymer composite is prepared by solvent evaporation method. For comparation, graphene/fluoropolymer biphase composite is also tested. Fig. 6c and 6d shows the representative SEM images of graphene/fluoropolymer biphase composite and graphene/MWCNTs/fluoropolymer composite used in this work. It can be found that graphene particles are prone to aggregation in graphene/fluoropolymer biphase composite. With the presence of MWCNTs, graphene particles are fairly well dispersed in the graphene/MWCNTs/fluoropolymer nanocomposite.

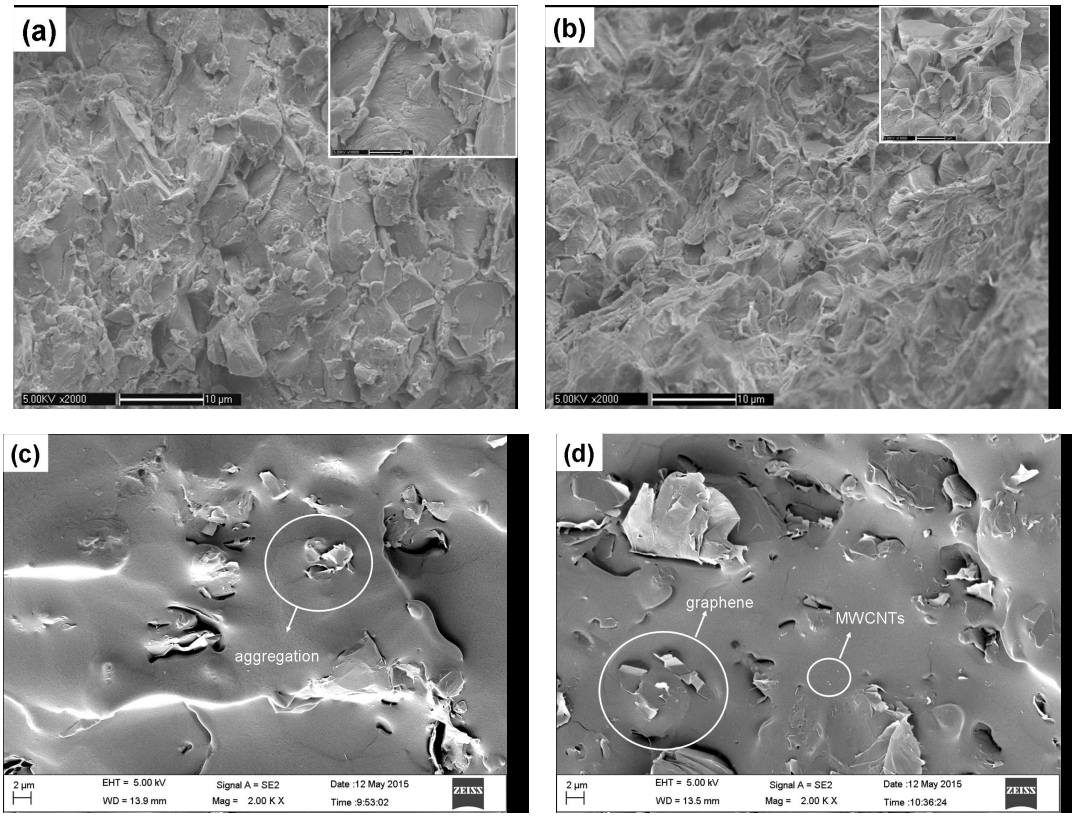

Fig. 6 SEM images of the fracture surface: (a) PBX-A; (b) PBX-B; (c) graphene/fluoropolymer composite; (d) graphene/MWCNTs/fluoropolymer nanocomposite.

3.4 Experimental description of the short time creep behaviors

3.4.1 Stress dependence

The creep compliance curves as a function of time during creep tests at three different testing stresses of the TATB-based PBX specimens without and with nanofillers are shown in Fig. 7. For the specimens studied here, under a low stress of 4 MPa, the creep compliance-time diagrams give very good linear relationships for all of the samples at the linear regime. Under higher stresses of 7 and 9 MPa, nonlinear viscoelastic regime, during which the creep compliance rate increases with creep time and creep rupture occurs, could be distinctly observed.

It can be found that at each testing stress, the creep compliance reduce and creep failure time prolongs with the incorporation of hybrid graphene/MWCNTs particles, revealing that the

nanofillers have an important effect on the creep deformation ability. The highest creep strain is observed for TATB-based PBX without nanofillers. As expected, the PBX-B filled with hybrid graphene/MWCNTs gives the lowest creep strain. The creep strain values of the graphene modified nanomaterials are intervenient between the values of PBX-A and PBX-B. The dispersion of nanoparticles and interfacial zones are considered here as crucial factors for the improvement in the creep resistance. Furthermore, the creep responses of TATB-based PBXs show obvious differences at the different applied stresses. As expected, high loading stress provides a significant reduction in the creep failure time and an increase in the creep compliance. In Fig 7a, it is obvious that the linear regime is below 7 MPa. And in Fig 7b and 7c, the linear regime is between 7 and 9 MPa. So the addition of hybrid graphene/MWCNTs or graphene particles increases the linear viscoelastic regime of the composite materials.

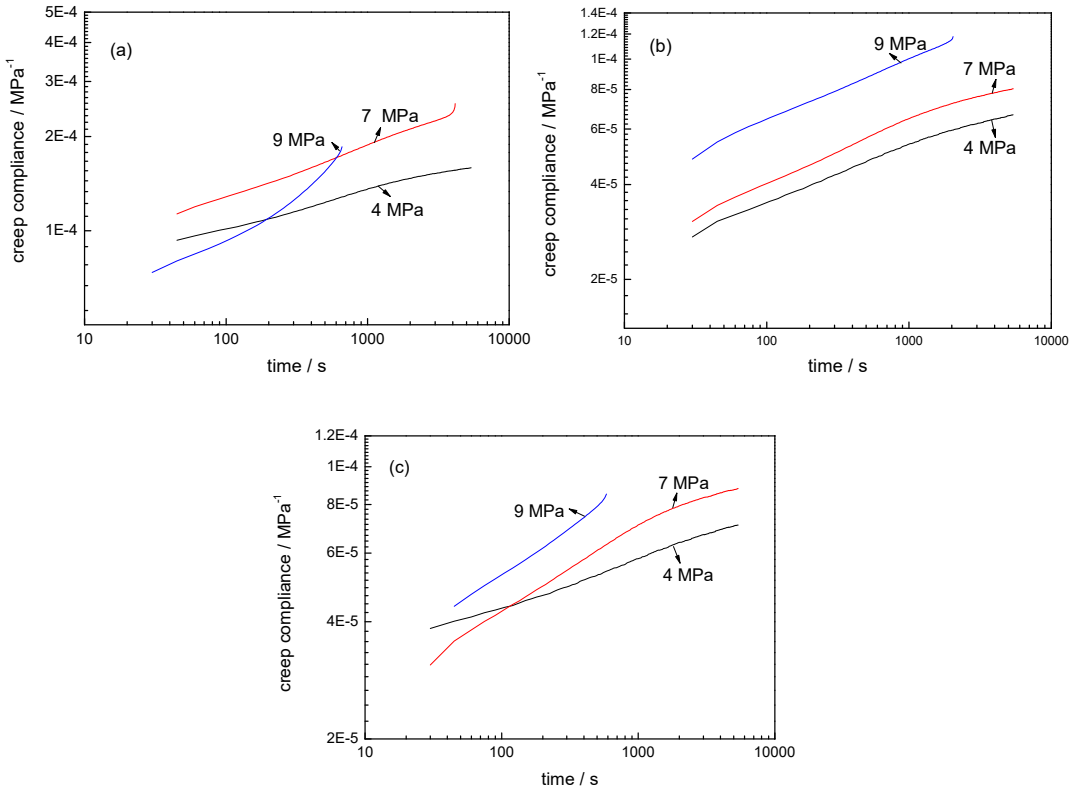

Fig. 7 Time-dependent creep compliance of TATB-based PBXs under different stresses at 60 °C: (a) PBX-A, (b) PBX-B, (c) PBX-C.

3.4.2 Temperature dependence

In addition, the creep compliance increases regularly with the increasing temperature, as given in Fig 8. High temperature can bring large creep compliance and accelerate the deformation of polymer materials. The creep compliance of the PBX-B at all test temperatures is lower than that of PBX-A, indicating a good creep resistance.

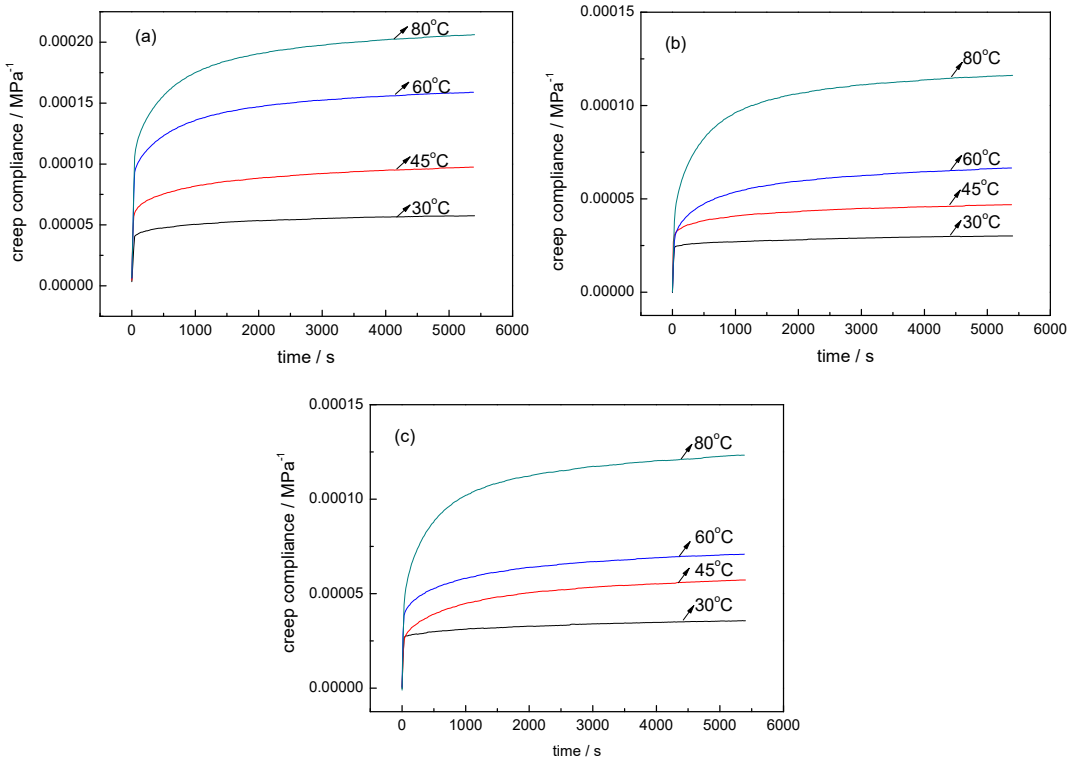

Fig. 8 Time-dependent creep compliance of TATB-based PBXs at different temperatures under 4 MPa: (a) PBX-A, (b) PBX-B, (c) PBX-C.

The increscent trend of creep resistance may be related to 3D MWCNTs/graphene hybrid architectures[35]. Two possible mechanisms to explain the synergetic enhancement of MWCNTs/graphene for polymer composites are proposed by Yang et al.[25] which are (i) flexible MWCNTs can construct graphene to form 3-D hybrid structure, which inhibit face to face aggregation of multi-graphene platelets. This results in a large surface area, so, increasing the contact surface area between MWCNTs/graphene and polymer matrix; (ii) the MWCNTs can act as extended tentacles for the 3-D hybrid architectures, which can become entangled with the polymer chain resulting better interaction between MWCNTs/graphene and the polymer matrix. A creep mechanism of PBX has been studied from the theory of deformation and sliding of molecular chain of the polymer by Ding et al.[36] It is shown that the creep property of the polymer is the main factor influencing on the creep-damage properties of the composite though polymer content is so little in amount. For TATB-based PBXs with MWCNTs/graphene hybrid nanocomposites studied here, the molecular motion of polymer binder system plays a crucial role in the creep resistance. Fig. 9 shows a diagram of formation of the MWCNTs/graphene 3-D hybrid structure in PBX. Because of the large Vander Waals forces and strong π-π interactions between nanosheets, graphene forms aggregations in PBX-C with graphene nanofillers, as shown in Fig. 9c. The incorporation of MWCNTs can effectively inhibit the stacking of graphene sheets and thus 3-D hybrid structure is constructed in the PBX-B with graphene/MWCNTs. The improved dispersion behavior of the graphene nanosheet by the addition of MWCNTs leads to a huge interphase between MWCNTs/graphene and polymer matrix and thus effectively restrict the motion of polymer chains. The modified load transfer from the polymer matrix to MWCNTs/graphene particles is influenced at the nanoscale, contributing to the observed enhancement of creep resistance for TATB-based PBXs.

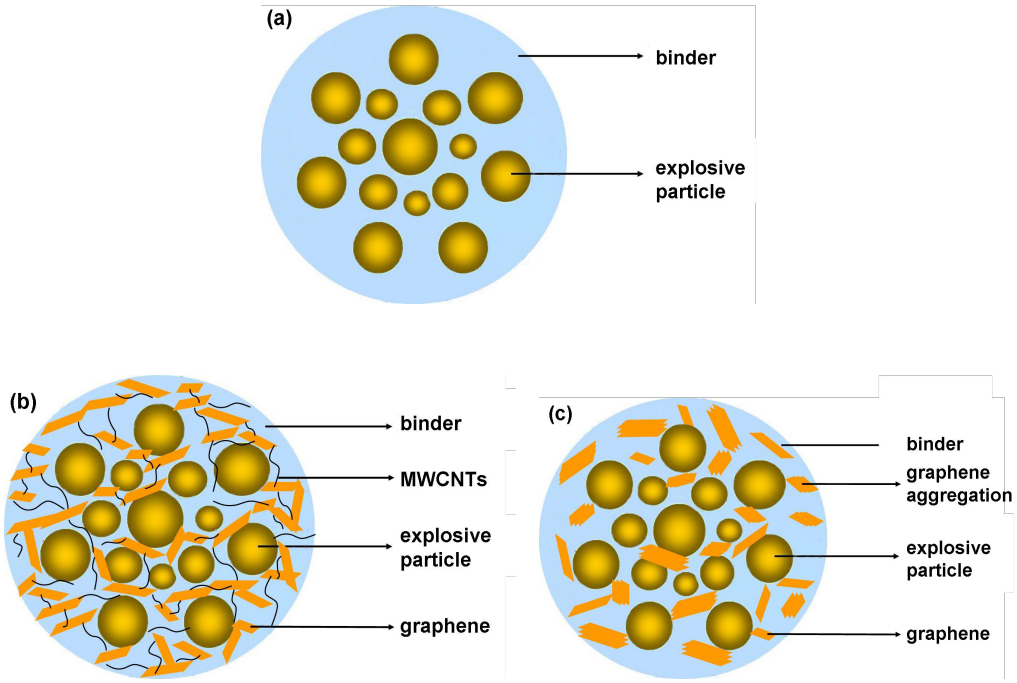

Fig. 9 The model of microstructural scheme of TATB-based PBXs: (a) PBX-A; (b) PBX-B; (c) PBX-C.

3.4.3 Creep modeling

As a combination of a Maxwell element and two Kelvin elements in series, the six-element mechanical model gives a good description of the experimental values of the creep compliance for TATB-based PBXs. Figure 10 illustrates the six-element mechanical model in which the elastic element is represented by a spring and the viscous element is represented by a dashpot. The total strain (ε) is the sum of instantaneous elastic deformation (ε_1), high elastic deformation (ε_2 and ε_3), and viscous flow (ε_4), given by:

$$\varepsilon(t) = \varepsilon_1 + \varepsilon_2 + \varepsilon_3 + \varepsilon_4 = \frac{\sigma_0}{E_1} + \frac{\sigma_0}{E_2}\left(1 - e^{-t/\tau_2}\right) + \frac{\sigma_0}{E_3}\left(1 - e^{-t/\tau_3}\right) + \frac{\sigma_0}{\eta_4}t \qquad (1)$$

where ε(t) denotes a function of creep strain ε with creep time t, σ_0 is the initial stress, E_1 is the elastic modulus of instantaneous elastic deformation, E_2 and E_3 are the elastic modulus of high elastic deformation, τ_2 and τ_3 are the relaxation time, η_4 is the bulk viscosity, respectively.

Equation 1 divides by σ_0:

$$\frac{\varepsilon(t)}{\sigma_0} = \frac{1}{E_1} + \frac{1}{E_2}\left(1 - e^{-t/\tau_2}\right) + \frac{1}{E_3}\left(1 - e^{-t/\tau_3}\right) + \frac{1}{\eta_4}t \qquad (2)$$

During the creep process, the loading stress is regarded as a constant value, and therefore, the creep process can be also characterized with the creep compliance D. The creep compliance can be calculated as:

$$D(t) = \frac{\varepsilon(t)}{\sigma} \qquad (3)$$

Equation 2 is transferred to creep compliance equation:

$$D(t)=\frac{1}{E_1}+\frac{1}{E_2}\left(1-e^{-t/\tau_2}\right)+\frac{1}{E_3}\left(1-e^{-t/\tau_3}\right)+\frac{1}{\eta_4}t \quad (4)$$

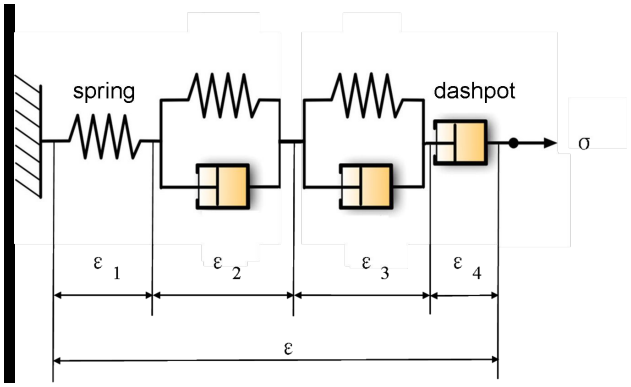

Fig. 10 Schematic representation of the six-element mechanical model.

The nonlinear curve fit results according to six-element mechanical model together with the regression coefficient, are shown in Fig. 11. From the figure, it can be seen that the mathematical formula fits well with the creep compliance for TATB-based PBXs at constant sustained load. The nonlinear regression coefficient (R^2), being in most cases higher than 0.994, also shows a good nonlinear correlation.

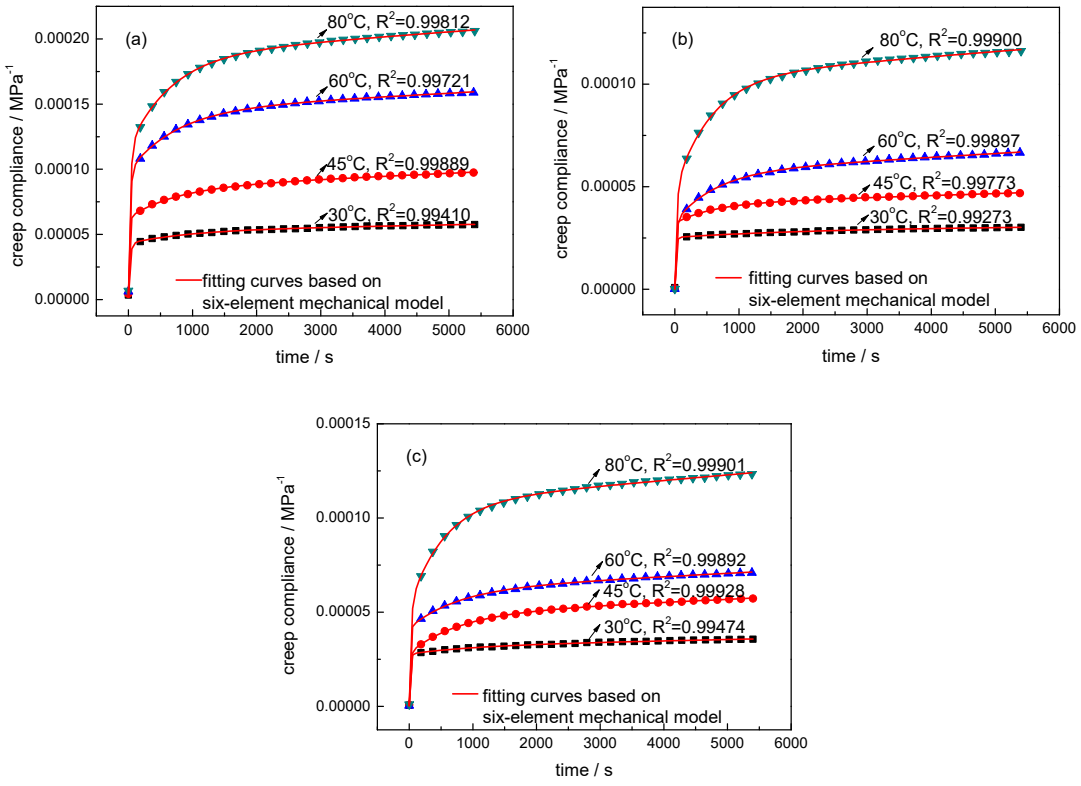

Fig. 11 Modeling results of creep behaviors of TATB-based PBXs at different temperatures under 4 MPa: (a) PBX-A, (b) PBX-B, (c) PBX-C.

The values of six fitting parameters including the elastic modulus E_1, E_2, E_3, the relaxation time τ_2, τ_3, as well as the bulk viscosity η_4 of TATB-based PBXs which are obtained from the nonlinear fitting curves are listed in Table 1. The values of E_2, E_3 and η_4 tend to increase with decreasing temperature and the addition of hybrid graphene/MWCNTs particles. The increased trend of E_2, E_3, and η_4 indicates the reinforced mechanical properties of the amorphous regions and increased resistance to viscous flow.

Table 1 The fitting parameters of six-element model under different conditions.

sample	test condition	E_1 /MPa	E_2 /MPa	τ_2 /s	E_3 /MPa	τ_3 /s	η_4 /MPa·s
PBX-A	30°C/4MPa	5.760×10^5	9.999×10^4	974.50	2.419×10^4	25.08	1.150×10^9
	45°C/4MPa	2.720×10^5	4.359×10^4	745.24	1.723×10^4	15.52	4.394×10^8
	60°C/4MPa	4.431×10^5	2.128×10^4	734.98	1.043×10^4	24.82	3.779×10^8
	80°C/4MPa	5.341×10^5	1.403×10^4	665.43	8.773×10^3	28.96	2.727×10^8
PBX-B	30°C/4MPa	2.312×10^6	2.422×10^5	2186.96	4.030×10^4	15.82	4.700×10^9
	45°C/4MPa	3.007×10^6	1.058×10^5	598.37	3.138×10^4	9.04	9.984×10^8
	60°C/4MPa	9.253×10^5	4.143×10^4	637.88	3.055×10^4	22.51	5.430×10^8
	80°C/4MPa	2.468×10^7	1.819×10^4	574.49	2.067×10^4	28.42	4.001×10^8
PBX-C	30°C/4MPa	5.525×10^6	2.360×10^5	1023.62	3.630×10^4	15.20	1.417×10^9
	45°C/4MPa	1.581×10^6	4.837×10^4	784.67	3.615×10^4	18.63	6.361×10^8
	60°C/4MPa	2.137×10^6	4.921×10^4	752.62	2.435×10^4	13.90	5.711×10^8
	80°C/4MPa	1.567×10^6	1.811×10^4	547.10	1.912×10^4	25.86	3.396×10^7

4. Conclusions

Non-linear time dependent viscoelastic behaviors of 1,3,5-triamino-2,4,6-trinitrobenzene (TATB)-based polymer bonded explosives (PBXs) modified by hybrid graphene/multiwalled carbon nanotubes (MWCNTs) were investigated and discussed in relation to the structural characteristics determined by SEM. Reference raw TATB-based PBX samples without nanofiller and with individual graphene were also tested and compared with the results obtained from the hybrid graphene/MWCNTs reinforced PBX. The nanocomposites filled with hybrid graphene/MWCNTs outperformed raw TATB-based PBX without nanofillers in respect to the storage modulus, compressive and tensile strength, elongation at break, and fracture energy. In addition, compared with raw TATB-based PBX without nanofillers, the creep compliance were reduced apparently for hybrid graphene/MWCNTs reinforced PBX with prolonged creep failure time this indicated a higher resistance of creep deformation. It was attributed to the better dispersion of graphene nanoparticles and higher interfacial zones with the incorporation of MWCNTs, which resulted in a restriction of the mobility of polymer chains. Taking into consideration these results, the addition of hybrid graphene/MWCNTs filler provides an efficient route for the improvement of non-linear viscoelastic properties of PBXs.

Acknowledgement

The authors are grateful to the Science and Technology Fund of CAEP (2015B0101011 and

2012A0201007) and National Natural Science Foundation of China (11372290 and 11502245) for financial support.

References

1. K. S. Novoselov, A. K. Geim, S. V. Morozov, D. Jiang, Y. Zhang, S. V. Dubonos, I. V. Grigorieva, and A. A. Firsov, Science, 2004, 306, 666-669.
2. A. K. Geim and K. S. Novoselov, Nat. Mater., 2007, 6, 183-191.
3. M. Mirnezhad, M. Modarresi, R. Ansari, and M. R. Roknabadi, J. Therm. Stresses, 2012, 35, 913-920.
4. L. Liu,Y. Gao, Q. Liu, J. Kuang, D. Zhou, S. Ju, B. Han, and Z. Zhang, Small, 2013, 9, 2466-2472.
5. R. J. Young, I. A. Kinloch, L. Gong, and K. S. Novoselov, Compos. Sci. Technol., 2012, 72, 1459-1476.
6. R. Gu, W. Z. Xu, and P. A. Charpentier, Polymer, 2014, 55, 5322-5331.
7. C. Heo, H. Moon, C. S. Yoon, and J. Chang, J. Appl. Polym. Sci., 2012, 124, 4663-4670.
8. A. Ranade, K. Nayak, D. Fairbrother, and N. A. D'Souza, Polymer, 2005, 46, 7323-7333.
9. S. Siengchin and J. Karger-Kocsis, Macromol. Rapid Comm., 2006, 27, 2090-2094.
10. J. L. Yang, Z. Zhang, K. Friedrich, and A. K. Schlarb, Macromol. Rapid Comm., 2007, 28, 955-961.
11. Y. Jia, K. Peng, X. L. Gong, and Z. Zhang, Int. J. Plasticity, 2011, 27, 1239-1251.
12. H. Varela-Rizo, M. Weisenberger, D. R. Bortz, and I. Martin-Gullon, Compos. Sci. Technol., 2010, 70, 1189-1195.
13. F. Bondioli, A. Dorigato, P. Fabbri, M. Messori, and A. Pegoretti, J. Appl. Polym. Sci., 2009, 112, 1045-1055.
14. H. Münstedt, T. Köppl, and C. Triebel, Polymer, 2010, 51, 185-191.
15. A. Zandiatashbar, C. R. Picu, and N. Koratkar, Small, 2012, 8, 1676-1682.
16. L. Tang, X. Wang, L. Gong, K. Peng, L. Zhao, Q. Chen, L. Wu, J. Jiang, and G. Lai, Compos. Sci. Technol., 2014, 91, 63-70.
17. X. Wang, L. Gong, L. Tang, K. Peng, Y. Pei, L. Zhao, L. Wu, and J. Jiang, Compos. Part A: Appl. Sci. Manuf., 2015, 69, 288-298.
18. J. A. King, D. R. Klimek, I. Miskioglu, and G. M. Odegard, J. Appl. Polym. Sci., 2013, 128, 4217-4223.
19. Y. Si and E. T. Samulski, Chem. Mater., 2008, 20, 6792-6797.
20. D. Li, M. B. Muller, S. Gilje, R. B. Kaner, and G. G. Wallace, Nat. Nanotech. 2008, 3, 101-105.
21. K. A. Worsley, I. Kalinina, E. Bekyarova, and R. C. Haddon, J. Am. Chem. Soc., 2009, 131, 1253-1255.
22. V. Datsyuk, M. Kalyva, K. Papagelis, J. Parthenios, D. Tasis, A. Siokou, I. Kallitsis, and C. Galiotis, Carbon, 2008, 46, 833-840.
23. M. T. Hung, O. Choi, Y. S. Ju, and H. T. Hahn. Appl. Phys. Lett., 2006, 89, 023117/1-3.
24. S. Y. Yang, C. C. M. Ma, C. C. Teng, Y. W. Huang, S. H. Liao, Y. L. Huang, H. W. Tien, T. M. Lee, and K. C. Chiou, Carbon, 2010, 48, 592-603.
25. S. Yang, W. Lin, Y. Huang, H. Tien, J. Wang, C. M. Ma, S. Li, and Y. Wang, Carbon, 2011, 49, 793-803.

26. S. Araby, N. Saber, X. Ma, N. Kawashima, H. Kang, H. Shen, L. Zhang, J. Xu, P. Majewski, and J. Ma, Mater. Des., 2015, 65, 690-699.
27. A. S. Patole, S. P. Patole, S. Y. Jung, J. B. Yoo, J. H. An, and T. H. Kim, Eur. Polym. J., 2012, 48, 252-259.
28. C. Lin, S. Liu, X. Tu, Z. Huang, Y. Li, L. Pan, and J. Zhang, Propell. Explos. Pyrot., 2015, 40, 189-196.
29. C. Lin, S. Liu, Z. Huang, G. He, F. Gong, Y. Liu, and J. Liu, RSC Adv., 2015, 5, 30592-30601.
30. C. Lin, J. Liu, F. Gong, G. Zeng, Z. Huang, L. Pan, J. Zhang, and S. Liu, RSC Adv., 2015, 5, 21376-21383.
31. C. Lin, J. Liu, G. He, L. Chen, Z. Huang, F. Gong, Y. Liu, and S. Liu, RSC Adv., 2015, 5, 35811-35820.
32. A. C. Ferrari and J. Robertson, Phys. Rev. B: Condens. Matter Mater. Phys., 2000, 61, 14095-14107.
33. A. C. Ferrari, J. C. Meyer, V. Scardaci, C. Casiraghi, M. Lazzeri, F. Mauri, S. Piscanec, D. Jiang, K. S. Novoselov, S. Roth, and A. K. Geim, Phys. Rev. Lett., 2006, 97, 187401/1-4.
34. M. Wen, H. Pang, M. Tang, W. Tang, and C. He, Chinese J. Energ. Mater., 2015, 23, 351-355.
35. M. Y. Yen, M. C. Hsiao, S. H. Liao, P. Liu, H. M. Tsai, C. C. M. Ma, N. W. Pu, and M. D. Ger, Carbon, 2011, 49, 3597-3606.
36. Y. Ding, Y. Pan, R. Cai, X. Yu, and Y. Yang, Chinese J. Energ. Mater., 2000, 8, 87-90.
37. F. Achereiner, K. Engelsing, M. Bastian, and P. Heidemeyer, Polym. Test., 2013, 32, 447-454.